

## LABORATORY EVALUATION OF WATERFLOOD RESIDUAL OIL SATURATION IN FOUR CARBONATE CORES

Jairam Kamath, Frank Nakagawa, Robert Meyer,  
Shah Kabir, and Randall Hobbet, Chevron

### ABSTRACT

Laboratory determination of residual oil saturation (ROS) in carbonate cores is sometimes uncertain due to wide pore size distribution, core scale heterogeneity, and complex wettability. The values obtained in laboratory tests may vary depending on flow rates, the type of samples (plugs or whole cores), and sample preparation techniques.

The purpose of our study is to integrate modern flow visualization technology with conventional laboratory tools to provide a comprehensive picture of waterflood recovery behavior in four carbonate cores. Our data set comprise thin sections; mercury injection; 3-D porosity distribution; oilfloods and waterfloods on cleaned samples; and 3-D flow imaging of miscible floods, oilfloods, and waterfloods on restored state samples.

The 3-D Computed Tomography (CT) images allowed us to understand the reasons for decrease in oil saturation observed with increased pressure drop in the corefloods; whether this is due to capillary-end effects, core scale heterogeneity, or actual reduction in ROS. We find that ROS values under field-rate flooding conditions ( $\sim 1$  psi/foot,  $N_c \bullet \sim 10^{-8}$ , lateral flood) are in the 30%-60% PV range. These ROS values reduce significantly as the pressure gradient applied during the floods is raised from field values to the much higher-pressure gradients sometimes used in laboratory testing ( $\sim 100$  psi/ft,  $N_c \sim 10^{-6}$ ). The carbonate samples with large pore-throat aspect ratios have the largest ROS values and the biggest variation with the pressure drop used in the waterfloods.

### INTRODUCTION

Carbonate rocks often display heterogeneities significant at the core plug scale (Narayanan and Deans, 1988, Hicks et.al., 1992, Moctezuma-B and Fleury; 1999, Siddiqui, Funk, and Khamees, 2000). Conventional analysis is likely to be inadequate for such rock systems (Ehrlich, 1971, McCaffery et.al., 1977, Archer and Wong, 1976, MacAllister et.al., 1993, Espie et.al., 1996). A review of studies on carbonate systems by Espie et al., 1996, shows a wide range of process efficiency. They find that the residual oil saturation to water flood varies from 28 to 80% oip and that to tertiary miscible flood varies from 0 to 50% oip.

deZabala and Kamath, 1995, used CT scanning to study a dolomite rock from the Beaverhill Lake formation, Canada ( $k=300$ md,  $\phi=14\%$ ). The porosity of this rock was predominantly intercrystalline, and thin section analysis shows millimeter size pore features. The remaining oil saturation in the dolomite sample varied from 67% pv to 37% pv when the waterflood rate was changed from the reservoir rate of 0.5 feet/day to the 120 feet/day recommended for conventional laboratory testing (Mohanty and Miller, 1991). CT

---

\* The capillary number,  $N_c$ , is the dimensionless ratio of viscous to capillary forces at the pore

level  $N_c = \frac{.01 \text{ mm}}{s}$ ; .01 is a conversion constant used to make  $N_c$  dimensionless using the units defined in the Nomenclature section.

images showed that the reduction in remaining oil saturation was due to unswept areas of the core being invaded as the flow rate was increased.

Given these uncertainties, we use CT visualization in this study to better understand displacement behavior in four carbonate cores.

## **EXPERIMENTAL PROCEDURE**

We followed the following testing sequence --

*Sample Selection* -- Select four whole core (dry, unpreserved) samples that represent different rock types. Clean using extended (> 10 cycles, each cycle > 3PV) flushes of toluene and methanol. Follow with extended (>30 PV) of chloroform:methanol. Measure  $K_{air}$  and  $\phi$ .

*Displacement Tests on Cleaned Samples* -- Vacuum saturate with 3% KCl. Conduct spontaneous imbibition tests and gravity-stabilizing displacements (refined oil->water and water-> refined oil) at different flow rates.

*Core Characterization* -- Re-clean core samples. Vacuum dry<sup>1</sup> and CT scan. Saturate with 11% KCl. CT scan and generate 3-D porosity distribution. Conduct a unit mobility, equal density miscible flood (10% KBr displacing 11% KCl) and use CT scanning to map permeability pathways. Use core end pieces to measure mercury injection data and to make thin section images.

*Unsteady State Tests on Restored State Samples* -- Displace 10% KBr with 1.6 cp refined oil. CT scan. Displace refined oil with crude oil and age for a minimum of 3 days<sup>2</sup> at 260 degF and 1000 psi. Flush with refined oil. CT scan. Flood with 10% KBr at reservoir flow rates (~ 1 foot/day). CT scan at intermediate times. After oil production has stopped, increase flow rate in steps to 5, 20, and 100 feet/day. CT scan at end of each rate bump.

*Steady State Tests on Restored State Samples* -- Miscibly clean sample using extended alternate flushes of toluene and methanol. Saturate with 10% KBr. CT Scan. Flood with refined oil. CT scan. Displace with crude oil and age for a minimum of 3 days at 260 degF and 1000 psi. Flush with refined oil. CT scan. Conduct steady state measurements with a total rate of ~ 10 feet/day and different fractional flows. CT scan at intermediate times. Miscibly clean and saturate with refined oil for base CT scan.

---

<sup>1</sup> All work after this point was conducted with the coreflood cell mounted in a horizontal position on the CT scanner table. We used a Technicare Deltascan 2020 HR scanner, maximum X-ray tube voltage - 120 Kev, tube current - 75 mA, beam thickness - 2 mm, 512 x 512 pixels, pixel size - 0.25 mm, scan time - 8 sec, and scan diameter - 12.7 mm.

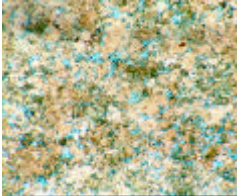

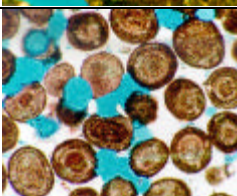
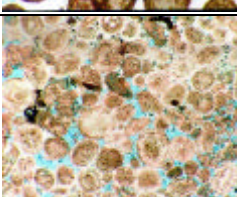
<sup>2</sup> Cuiec, 1991, has shown that 3 days aging is sufficient for carbonates.

## RESULTS

### *Sample Properties*

The vertical whole core samples were 2.125" in diameter and approximately 4" in length. Table 1 displays air permeability, porosity, geological descriptions and thin section images

--

| Sample | kbrine<br>(md) | f<br>(%) | Rock Type   | Thin Section  |
|--------|----------------|----------|---|---|
| K2     | 49             | 26       | Limestone micrite consists of 1-10 micrometer-size crystals of calcite with significant porosity between crystals. Pore body-throat ratio is probably close to unity. Homogeneous rock.   |    |
| K3     | 12             | 20       | Heterogeneous compound limestone with peloid-skeletal packstone to wackestone and skeletal-intraclast-oid packstone to grainstone textures with moldic, microcrystalline, and chalky intraparticle porosity.                              |    |
| K4     | 6              | 17       | Oolitic limestone with grainstone texture and abundant calcite cement. Cement is heterogeneously distributed. Pore body-throat ratio is quite large with pore bodies 200-400 micrometers across and pore throats a few micrometers across |   |
| K5     | 85             | 24       | Heterogeneous, compound limestone with grainstone texture and abundant calcite cement. The interparticle porosity is occluded with later, pore-filling cement. Pore body-throat ratio is probably large, but not as large as in K4.       |  |

**Table 1: Air permeability, porosity, geological descriptions and thin section images**

Figure 1 compares the pore throat radii distributions calculated from mercury injection measurements on end pieces from the whole cores. Samples K2 and K5 have the highest porosity and permeability, and this is due to a significant portion of the pore space being in 5-30  $\mu\text{m}$  range. Following the classification scheme of Martin et.al, 1997, the middle figure reveals that K2 is macro-mesoport rock; K3 is mostly mesoport; K4 mostly microport; and K5 is mega-macroport rock with significant microporosity.

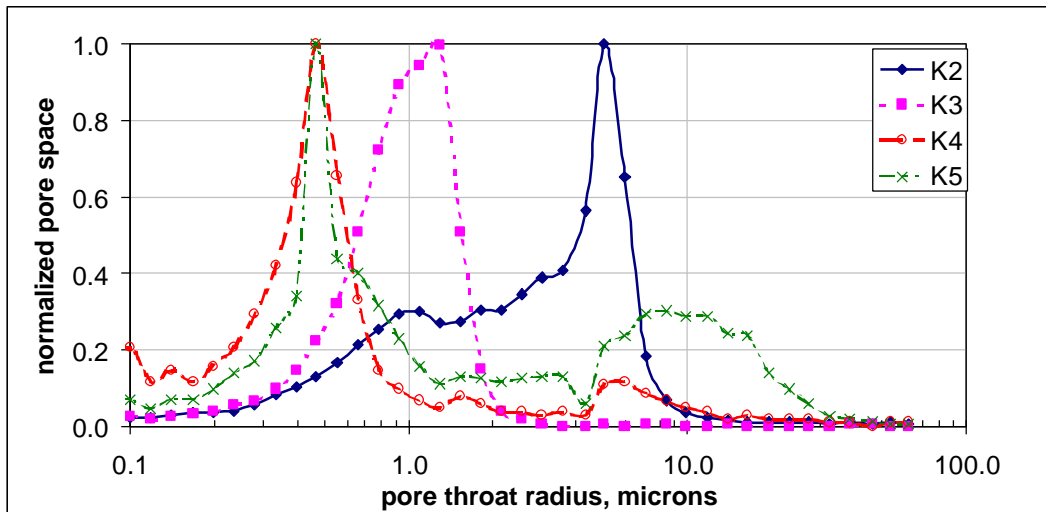


Figure 1: Pore throat size distributions

**Porosity and Permeability Distribution**

We used the difference in CT numbers between the dry and brine saturated cores to create 3-d porosity distributions for the core samples. Figure 2 shows CT images of typical porosity variation in a cross section perpendicular to flow. Structures in the porosity pattern are evident.

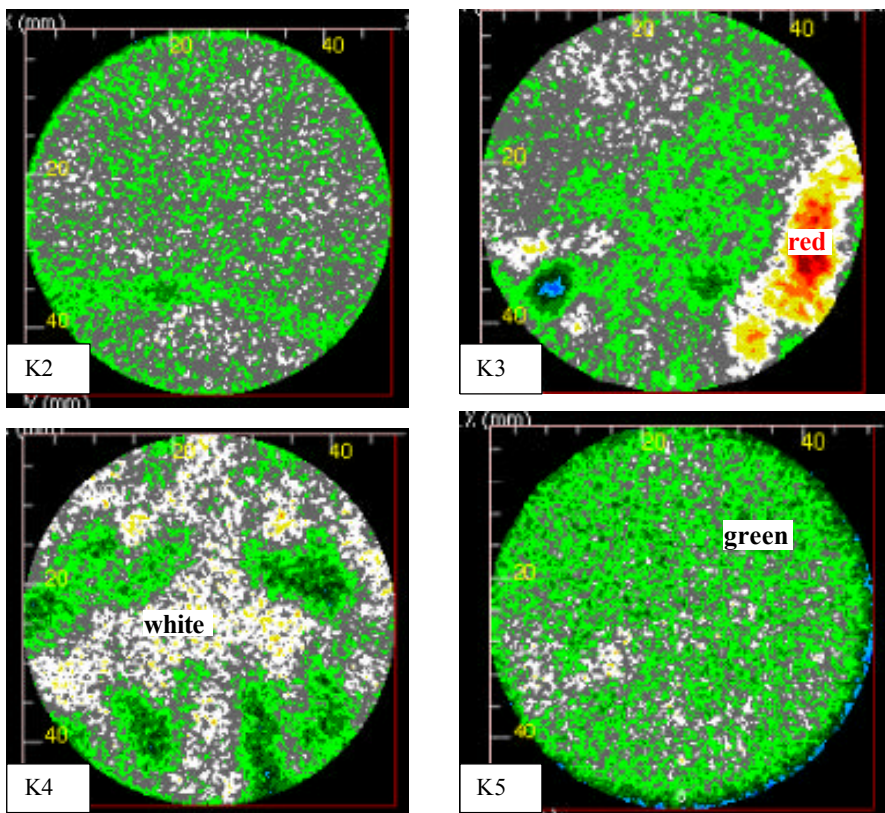


Figure 2 Porosity variation from CT scanning.  
 Color scale -- green :21%,grey:25%,white:29%,yellow:33%, red:40%

Figure 3 displays the brine concentration in a slice near the core inlet measured after injection of 0.4 pore volumes of 10% KBr (red) into 11% KCl (blue) saturated cores. This is a unit mobility, equal density, miscible displacement and is a good indicator of permeability heterogeneity. The CT images clearly show the different types of permeability structures in the four core samples. K2 is uniform; K3 has higher permeability towards the bottom of the core; K4 has local permeability heterogeneity but does not have correlated permeability regions; and K5 shows some spatial correlation in permeability paths.

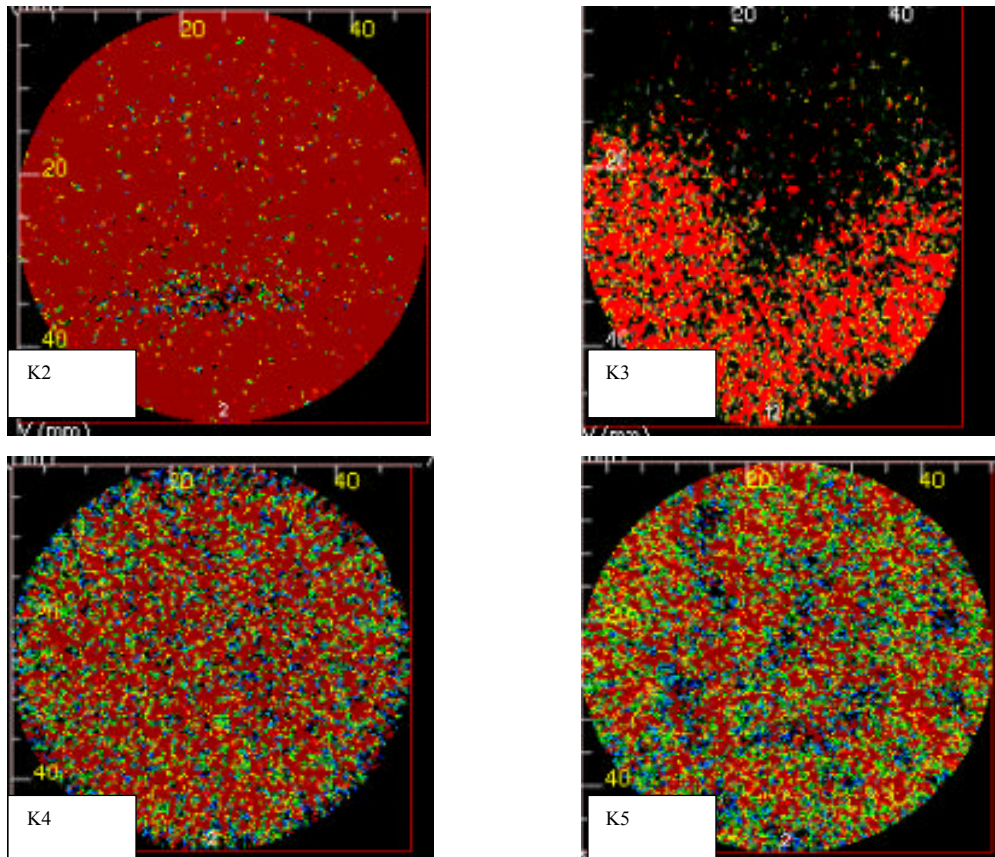


Figure 3: Brine concentration near inlet end during an unit mobility, equal density miscible flood. 0.4 PVI of KBr has been injected into KCl saturated cores. Red-KBr, blue—KCl.

Figure 4 plots the average in-situ concentration data from the miscible flood as a function of pore volumes of injected KBr. It reveals that sample K2 has low dispersivity (Brigham, 1974). This is consistent with the thin section and mercury injection data that show a homogeneous rock with narrow pore size distribution. Samples K3, K4 and K5 have very high dispersivity. This is consistent with the thin section and mercury injection data that show heterogeneous rocks (K3, K4, K5) and broad pore size distribution (K4, K5).



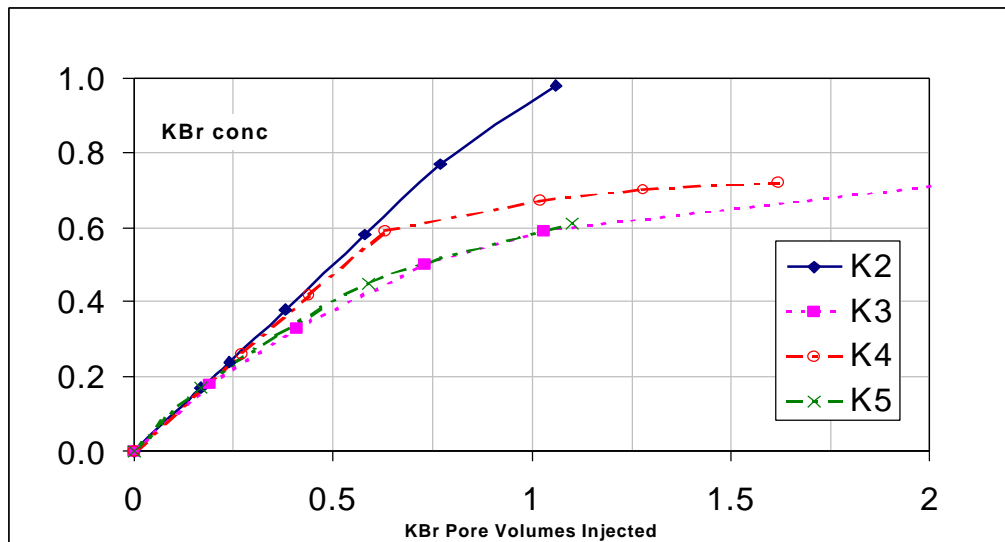


Figure 4: Experimentally measured in-situ KBr concentration – miscible flood KBr displacing KCl.

Figure 4 shows that sample K2 has low dispersivity ( $L/\alpha = 100$ ,  $L \sim 10$  cm  $\Rightarrow \alpha = 0.1$  cm). This is consistent with the thin section and mercury injection data that show a homogeneous rock with narrow pore size distribution. Samples K3, K4 and K5 have very high dispersivity ( $L/\alpha = 1$ ,  $L \sim 10$  cm  $\Rightarrow \alpha = 10$  cm). This is consistent with the thin section and mercury injection data that show heterogeneous rocks (K3, K4, K5) and broad pore size distribution (K4, K5). The dispersivity value should be used qualitatively, as the value is so large that it violates the assumptions behind the conventional dispersion-convection formulation used to describe the process.

**Primary Drainage**

All the samples have pore space in the sub-micron range (see figure 1) and this explains our difficulty in driving initial water saturation below 20% PV. Figure 5 plots the water saturation remaining in the core samples as a function of capillary number,  $N_c$ , and pressure gradient. These tests were conducted by flooding water-saturated cores with increasing flow rates of refined oil. We were able to reduce water saturation to 20% in samples K2, K3 and K4 by increasing the pressure drop to several hundred psi/foot. However, the water saturation in sample K5 at 400 psi/foot was 35%. This was unexpected as K5 is the highest permeability sample in this study. Perhaps the bimodal nature of the porosity distribution in sample K5 causes large amounts of water to be immobile.

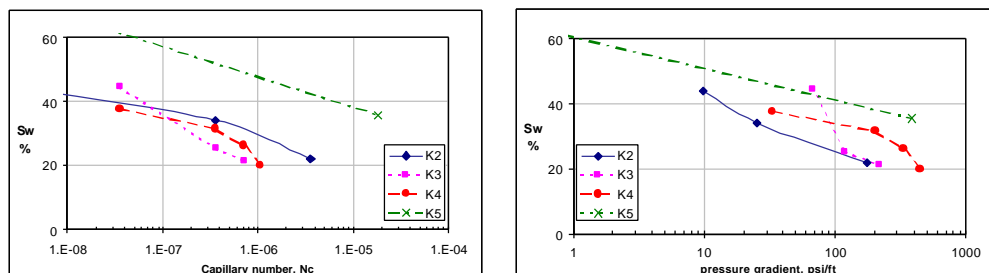


Figure 5: Initial water saturation is a strong function of the capillary number,  $N_c$ , or pressure gradient to which the cores are subject.

**Remaining oil saturation**

Figure 6 displays the remaining oil saturation in the cleaned and aged core samples at the end of the different rate waterfloods. This is not the same as residual oil saturation, ROS, as it is influenced by non-uniform oil saturation, core scale heterogeneity, and includes oil held up due to capillary end effects. It is a very strong function of the capillary number or pressure gradient during the floods. In addition, the data on unsteady state cleaned samples (■), unsteady state restored samples (○), and steady state restored samples (●) are consistent.<sup>3</sup>

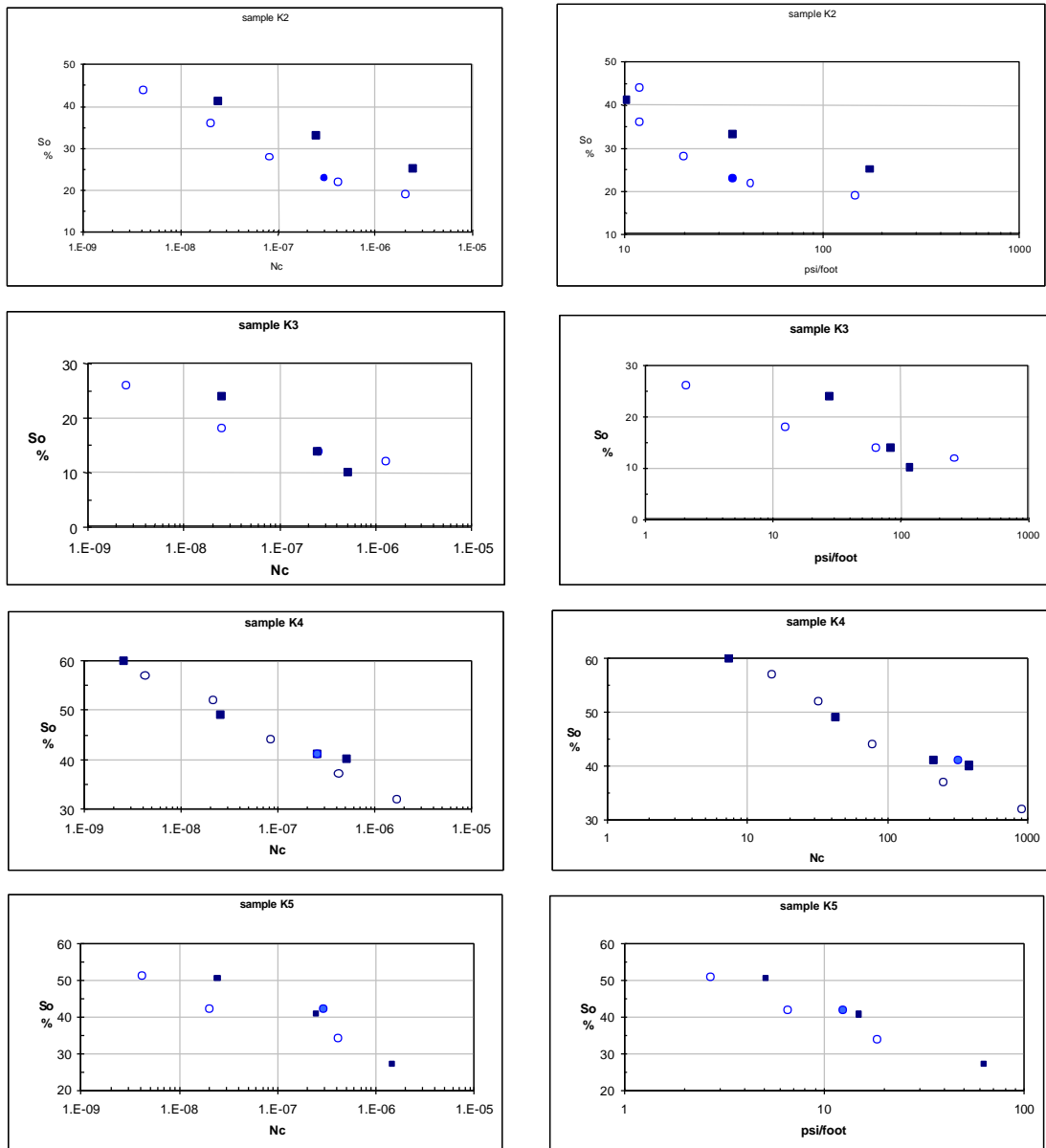


Figure 6: Remaining oil saturation as a function of capillary number (left) and pressure gradient (right). Key: Unsteady state cleaned (■), unsteady state restored state (○), and steady state (●)

<sup>3</sup> steady state remaining oil saturation defined at water fractional flow of 99.9%; some of the differences in absolute numbers at a given rate could be due to differences in initial water saturation

***Amott Wettability***

We measured Amott wettability only for the cleaned samples. We note here that the remaining oil saturation dependencies were similar for the restored state and cleaned samples. Table 2 shows that water Amott indices are close to zero, and oil Amott indices range from 0 to 0.3. All flood saturation values in Table 2 are the end points at the end of the highest rate flood. The duration of the imbibition tests varied from a few days to a few months.

|                           | <b>K2</b>   | <b>K3</b>   | <b>K4</b>   | <b>K5</b>   |
|---------------------------|-------------|-------------|-------------|-------------|
| Initial Sw                | 100         | 100         | 100         | 100         |
| Sw after OilFlood         | 22          | 21          | 20          | 24          |
| Sw after Water Imbibition | 22          | 23          | 22          | 25          |
| Sw after Water Flood      | 75          | 90          | 60          | 72          |
| Sw after Oil Imbibition   | 73          | 90          | 47          | 65          |
| Sw after OilFlood         | 26          | 20          | 16          | 39          |
| <b>Water Amott</b>        | <b>0.00</b> | <b>0.03</b> | <b>0.05</b> | <b>0.02</b> |
| <b>Oil Amott</b>          | <b>0.04</b> | <b>0.00</b> | <b>0.30</b> | <b>0.21</b> |

Table 2: Amott wettability indices for the cleaned samples

***Saturation Profiles from CT scanning -- Restored State Samples***

Figure 7 contains the CT derived<sup>4</sup> oil saturation profiles at the end of primary drainage ( $S_{oi}$ ) and at the end of the different rate waterfloods.  $S_{oi}$  was established in these cores by displacing a brine saturated core with a 1.5 cp refined oil at a low-pressure drop and then gradually increasing the pressure drop to 250 psi/foot. This procedure allowed us to reach a uniform saturation in all the cores except sample K5. We suspect this is due to the bimodal nature of this rock that does not allow us to remove water held in the smaller pores towards the outlet end of the rock.

The refined oil was then displaced by crude and the core was aged at 260 degF and 1000 psi for at least three days. The waterfloods were first conducted at a low-pressure gradient. At the end of this step, the pressure gradient was raised in steps to the values shown. The oil saturation decreases in all cores as the pressure gradient is increased. Sample K2 is the only sample that shows a clear capillary end effect. The oil held up towards the outlet end of the core reduces as the gradient is raised. We note here that 3-d images of the floods showed that there was no gravity override in these horizontal corefloods.

<sup>4</sup> CT derived saturation values were, on average, within 3 saturation units of material balance values.



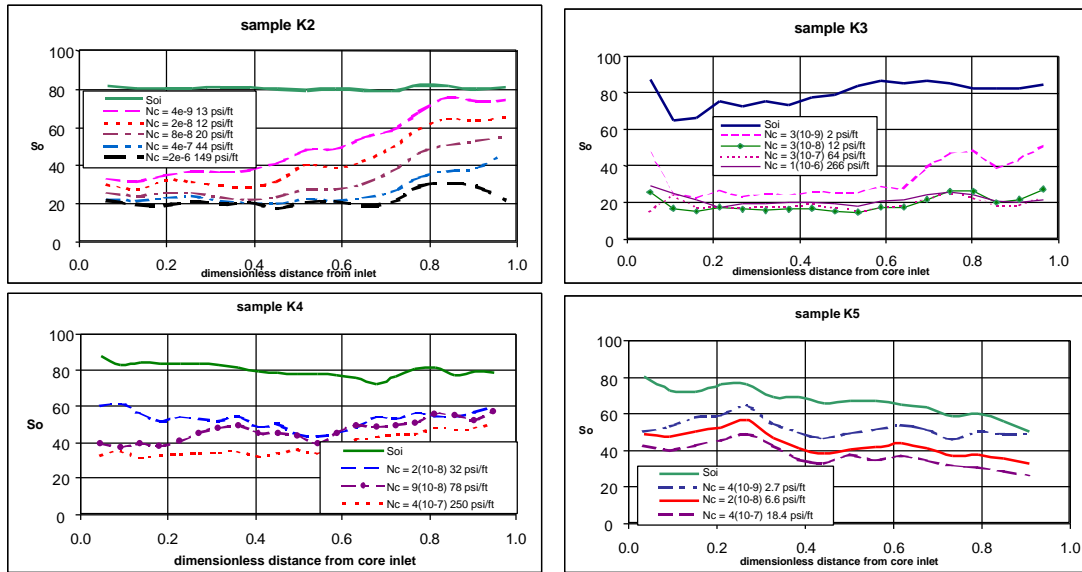


Figure 7: Oil Saturation profiles at end of different rate waterfloods

**Residual Oil Saturation, ROS**

We have presented results in an earlier section that showed the remaining oil saturation decreased with increasing pressure gradient applied during the corefloods. This data is influenced by non-uniform initial oil saturation, capillary end effects, and heterogeneity. We used local CT saturation data to remove some of these artifacts, and display ROS data in Figure 8. Samples K4 and K5 have the largest ROS values and the strongest dependency of ROS on pressure gradient. This corresponds well with the wide pore size distribution and the large pore body to pore throat aspect ratio of these samples.

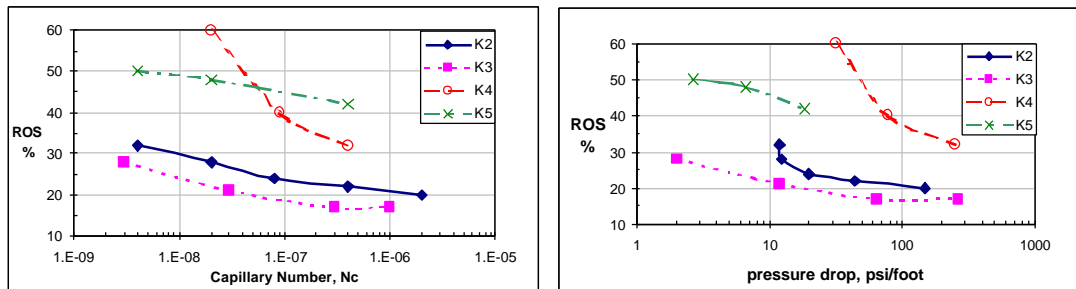


Figure 8: Variation in ROS with capillary number and pressure gradient -- restored state data. ROS data corrected for measurement artifacts;  $S_{oi} = 0.85$

**Steady State Data**

The steady state data were conducted on restored state samples at a single total flow rate of  $\sim 10$  feet/day, i.e.  $N_c \sim 4(10^{-7})$ . Figure 9 plots the saturation profiles at the various fractional flow of water,  $f_w$ . Sample K2 shows strong capillary end effects at high  $f_w$  values. The results of sample K5 are confounded by the non-uniform initial oil saturation profiles. The points (●) represent data measured during the unsteady state tests at  $S_{oi}$  and at the end of the waterflood at  $N_c \sim 4(10^{-7})$ . The figure reveals that the steady and unsteady state data correspond well.

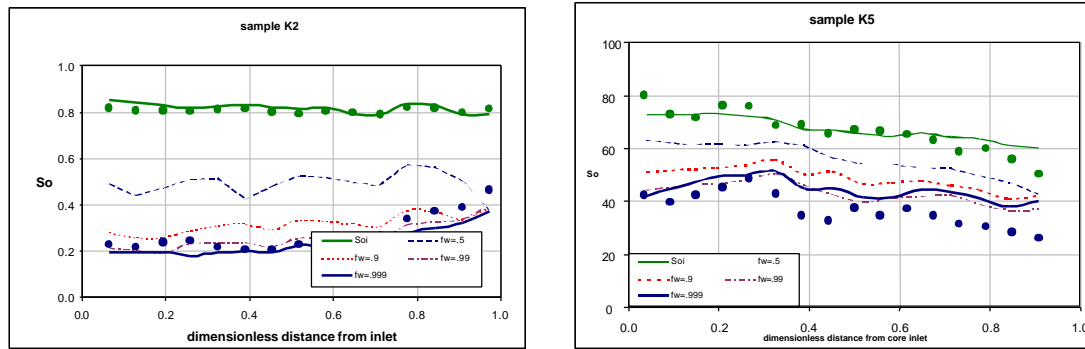


Figure 9: Oil saturation profiles. Lines represent steady state data conducted at  $N_c \sim 4(10^7)$  on restored state samples. The points (●) are unsteady state data at  $S_{oi}$  and at end of a waterflood at  $N_c \sim 4(10^7)$ .

## DISCUSSION

It is surprising to note the paucity of published data on flow-rate effects on ROS in carbonates. This may be due the difficulty in determining if additional oil production is due to reduction in capillary end effect, core scale bypassing, or ROS.

Abrams, 1975, studied 1 limestone sample and 6 water wet sandstones. Even though the limestone sample showed a continuous reduction in ROS from 34% pv to 17% pv when  $N_c$  was increased from  $10^{-7}$  to  $10^{-2}$ , he based his general conclusions on the behavior of the water-wet sandstone samples. Abrams states that the flow rate/ $N_c$  has to be increased by a factor of 100-1000 times above typical field rates before ROS will decrease.

There have been published reports of discrepancies between ROS values determined from unsteady state, steady state, and centrifuge tests. For example, Pham and Shari, 2001, report values of 10-35% pv from steady state, 28-46% from unsteady state, and 8-35% pv from centrifuge tests. They state that the centrifuge values may not represent the field conditions, essentially lateral flooding. Verma, Boucherit, and Bouvier, 1991, centrifuged carbonate cores after waterflooding and the ROS reduced from an average of 31% pv to 24% pv. They claimed that it was difficult to apply sufficient differential pressure in these high permeability rocks to reach the true ROS in this thick reservoir with strong gravity forces. They state that 24% pv is closer to the value measured in the field with logs. Unfortunately, these studies do not report flow rate or centrifuge speed information or any variation in these parameters to judge differences due to technique or due to balance of the viscous/capillary/gravity forces.

Mohanty and Miller, 1991, used flow visualization to convincingly show that mixed wet sandstones should show continuous reductions in ROS with flow rate. We have demonstrated that at least part of the oil production on increase of flow rate in these four carbonate cores is due to reduction in ROS. It appears that the concepts of critical capillary number to cause reductions in ROS (Abrams, 1975) are not valid for these carbonate rocks. Ideally, this type of data should be augmented by experiments that have different flow rates from the beginning of the test. Also, additional tests using a centrifuge are needed if gravity forces play an important role in ROS.

## SUMMARY

### *General*

1. Trends of average ROS with pressure gradient are similar for the cleaned and restored state samples. ROS values under field-rate flooding conditions are in the 30%-60% PV range.
2. Samples with large pore-throat aspect ratios have the largest ROS values and the biggest variation with the pressure drop used in the waterfloods.
3. For the cleaned samples, water Amott indices are close to zero and oil Amott indices range from 0 to 0.3.
4. Steady state and unsteady state saturation profiles are in reasonable agreement, and yield similar remaining oil saturation values.
5. Corefloods on carbonates should be conducted over a range of pressure gradients. If the data shows significant variation in remaining oil saturation, it is important to use flow visualization to understand the reasons.

### *By Sample*

1. Sample K2 (49 md, 26% porosity) is a limestone micrite, macro-mesoport rock, with pore-body throat ratio close to unity. Thin section and CT data revealed that it is homogeneous at the mm and cm scales. Waterfloods on the restored state sample showed the presence of a strong capillary end effect, with significant oil hold-up. ROS values decreased from 32% pv to 20% pv when the pressure gradient during the waterflood was raised from 12 to 150 psi/foot (Nc:  $4(10^{-9})$  to  $2(10^{-6})$ ).
2. Sample K3 (12 md, 20% porosity) is a compound limestone, mesoport rock with a narrow pore throat distribution. Thin section and CT data revealed that it is heterogeneous at the mm and cm scales. ROS values decreased from 28% pv to 17% pv when the pressure gradient during the waterflood was raised from 2 to 266 psi/foot (Nc:  $3(10^{-9})$  to  $1(10^{-6})$ ).
3. Sample K4 (6 md, 17% porosity) is an oolitic limestone, mostly microport rock with some bimodal porosity and a very large pore body-throat aspect ratio. CT data showed correlated permeability structures along the sample length. ROS values decreased from 60% pv to 32% pv when the pressure gradient during the waterflood was raised from 32 to 250 psi/foot (Nc:  $2(10^{-8})$  to  $4(10^{-7})$ ).
4. Sample K5 (85 md, 24% porosity) is a heterogeneous compound limestone, mega-macroport rock with significant microporosity, and has a fairly large pore body-throat aspect ratio. Miscible flood data showed correlated permeability structures along the sample length. There was significant water hold up due to capillary end effects during primary drainage. ROS values decreased from 50% pv to 42% pv when the pressure gradient during the waterflood was raised from 3 to 18 psi/foot (Nc:  $4(10^{-9})$  to  $4(10^{-7})$ ).

## ACKNOWLEDGEMENTS

We thank Ed deZabala and Russ Boyer for assistance with CT scanning and data collection, Jeff Warner for thin section descriptions, and John Popek for mercury injection data.

**NOMENCLATURE**

|          |   |                              |
|----------|---|------------------------------|
| k        | = | permeability, md             |
| $N_c$    | = | capillary number             |
| pv       | = | pore volume                  |
| S        | = | saturation, %                |
| v        | = | superficial velocity, cm/sec |
| $\sigma$ | = | interfacial tension, dyne/cm |
| $\mu$    | = | viscosity, cp                |

**Subscripts**

|   |   |            |
|---|---|------------|
| i | = | initial    |
| n | = | normalized |
| o | = | oil        |
| r | = | relative   |
| w | = | water      |

**REFERENCES**

Archer, J. S. and Wong, S. W.: "Use of a Reservoir Simulator to Interpret Laboratory Waterflood Data," *SPEJ* (February 1976)

Brigham, W. E.: "Mixing Equations in Short Laboratory Cores," *SPEJ* (Feb. 1974) 91-99.

Cuiec, L.: "Evaluation of Reservoir Wettability and its Effects on Oil Recovery," *Interfacial Phenomena in Oil Recovery*, N. R. Morrow (ed.). Marcel Dekker, Inc., 1991.

deZabala, E. F. and Kamath, J. : "Laboratory Evaluation of Waterflood Behavior of Vugular Carbonates," SPE 30780 presented at the 1995 SPE Annual Technical Conference and Exhibition, Dallas, October 22-25.

Ehrlich, R: "Relative Permeability Characteristics of Vugular Cores -- Their Measurement and Significance," paper SPE 3553 presented at the 46th Annual SPE of AIME Fall Meeting, New Orleans, LA, October 3-6, 1971.

Espie, A. A., Brown, C. E., Lamb, S. P. : "Near Miscible Gas Displacement in Vuggy Carbonates," paper SPE 35424 presented at the 1996 SPE/DOE Tenth Symposium on Improved Oil Recovery, Tulsa, April 21-24.

Hicks, P.J., Jr., Deans, H.A., and Narayanan, K.R.: "Distribution of Residual Oil in Heterogeneous Carbonate Cores Using X-ray CT," *SPEFE* (Sep. 1992) 235-240.

Lake, L. W. , *Enhanced Oil Recovery*, Prentice Hall, 1989, 163-168.

Martin, A. J., S. T. Solomon, and D. J. Hartmann, 1997, Characterization of Petrophysical Flow Units in Carbonate Reservoirs: *AAPG Bulletin* (May 1997) **V. 81**, No. 5, 734-759.

MacAllister, D.J., Miller, K.C., Graham, S. K., and Yang, C-T.: "Application of X-Ray CT Scanning To Determine Gas/Water Relative Permeabilities," *SPEFE* (Sep. 1993).

McCaffery, F. G., Sigmund, P.M., and Fosti, J. E. : "Pore Space and Displacement Characteristics of Carbonate Reservoir Rocks," Formation Evaluation Symposium of the Canadian Well Logging Society, Calgary, October 1977.

Narayanan, K. and Deans, H.A.: "A Flow Model Based on the Structure of Heterogeneous Porous Media," paper SPE 18328 presented at the 1988 SPE Annual Technical Conference and Exhibition, Houston, TX, Oct. 2-5,1988.

Moctezuma-B A., and Fleury, M. "Permeability Mapping on Vuggy Core Sample Using Tracer Experiments and Stream-Line Simulations," 1999 Society of Core Analysts International Symposium, Denver.

Mohanty, K.K. and Miller, A.E.: "Factors Influencing Unsteady Relative Permeability of a Mixed-Wet Reservoir Rock," *SPEFE* (Sep. 1991) 349-358.

Siddiqui, S., Funk, J. and Khamees, A. "Static and Dynamic Measurements of Reservoir Heterogeneities in Carbonate Reservoirs", 2000 Society of Core Analysts International Symposium, Abu Dhabi.